



Design, synthesis and photophysical properties of A-D-A-D-A small molecules for photovoltaic application



Weibo Yan^a, Qian Zhang^b, Qingsong Qin^a, Senyun Ye^a, Yuanwei Lin^a, Zhiwei Liu^a, Zuqiang Bian^{a,*}, Yongsheng Chen^b, Chunhui Huang^a

^a Beijing National Laboratory for Molecular Sciences, State Key Laboratory of Rare Earth Materials Chemistry and Applications, College of Chemistry and Molecular Engineering, Peking University, Beijing 100871, China

^b State Key Laboratory for Functional Polymer Materials and Center for Nanoscale Science & Technology, Institute of Polymer Chemistry, College of Chemistry, Nankai University, Tianjin 300071, China

ARTICLE INFO

Article history:

Received 1 April 2015

Received in revised form

25 April 2015

Accepted 7 May 2015

Available online 16 May 2015

Keywords:

Linear-conjugated small molecules

Acceptor-donor-acceptor-donor-acceptor

Hole mobility

Low bandgap

Solution processed

Organic solar cell

ABSTRACT

A series of linear-conjugated small molecule compounds featured with the acceptor-donor-acceptor-donor-acceptor (A-D-A-D-A) structure were designed, synthesized and characterized. The films of the compounds showed a broad UV–Vis absorption range of 300–800 nm with high molar absorption coefficient of more than $1.0 \times 10^4 \text{ cm}^{-1}$. Their hole-mobility can be as high as $1.0 \times 10^{-3} \text{ cm}^2 \text{ V}^{-1} \text{ s}^{-1}$. The compounds have a compatible HOMO energy level of -5.0 eV to PC₇₁BM and a high solubility up to 20 mg mL⁻¹ in chloroform. Therefore, compounds can blend with PC₇₁BM in the chloroform and form an active layer for a photovoltaic cell device by spin-coating of the blend solution. A maximum power conversion efficiency of 3.2% was achieved with the DERH3TT solar cell device. These results indicate that the A-D-A-D-A small molecules with electron-withdrawing dyes as terminals are promising candidates for the high efficiency solution processed organic photovoltaic cells.

© 2015 Elsevier Ltd. All rights reserved.

1. Introduction

Linear-conjugated small molecules have attracted considerable attentions recently due to their applications in many fields, such as in light-emitting diodes [1–5], thin-film transistors [6,7], as well as in organic photovoltaic (OPV) cells [8–25]. Generally, these conjugated small molecules prepared by rational molecular design contain finite conjugated units and are highly soluble in organic solvents. Therefore, their corresponding films can be formed simply by solution processing without the vacuum evaporation process that is required for the fabrications of most film devices [26]. These small molecules have an acceptor-donor-acceptor (A-D-A) or donor-acceptor-donor (D-A-D) structure, which is favorable for low bandgap molecules and low HOMO energy level with broad UV–Vis absorption range. In addition, due to their rigid structures and high mobility, the soluble small molecules can form a good phase-separated mixture as a donor with the acceptors such as [6,6]-phenyl-C₆₁-butyric acid methyl ester (PC₆₁BM) or [6,6]-

phenyl-C₇₁-butyric acid methyl ester (PC₇₁BM). All these unique properties of the linear-conjugated small molecules including high solubility, excellent light absorption ability, high hole-mobility and the compatible energy level and good phase-separation with PCBM contribute to their high performances in OPV cells.

The currently available single layer OPV devices with the solution-processed small molecules as donor active materials can show PCEs of >9% [25], which is comparable with that of the polymer counterparts [27]. Therefore, novel donor materials are very attractive for the preparation high efficiency solution processed organic photovoltaic cells. In the present work, we reported the design, synthesis and OPV performances five acceptor-donor-acceptor-donor-acceptor (A-D-A-D-A) small molecules including DERH3TT, DPRH3TT, DORH3TT, DPPR3TT and DBPPR3TT (Chart 1). Thienothiophene-one unit was chosen as the central building block due to its extendable conjugation and planar structure. In addition, this unit can form donor-acceptor-donor (D-A-D) structure with three thiophene units on both sides due to its weak electron-drawing property. This construction can lower the HOMO energy level and band-gap of the target molecules. Rhodanine and pyrazolone derivatives were selected as the terminal groups, which had been manifested to enhance the light

* Corresponding author.

E-mail address: bianzq@pku.edu.cn (Z. Bian).

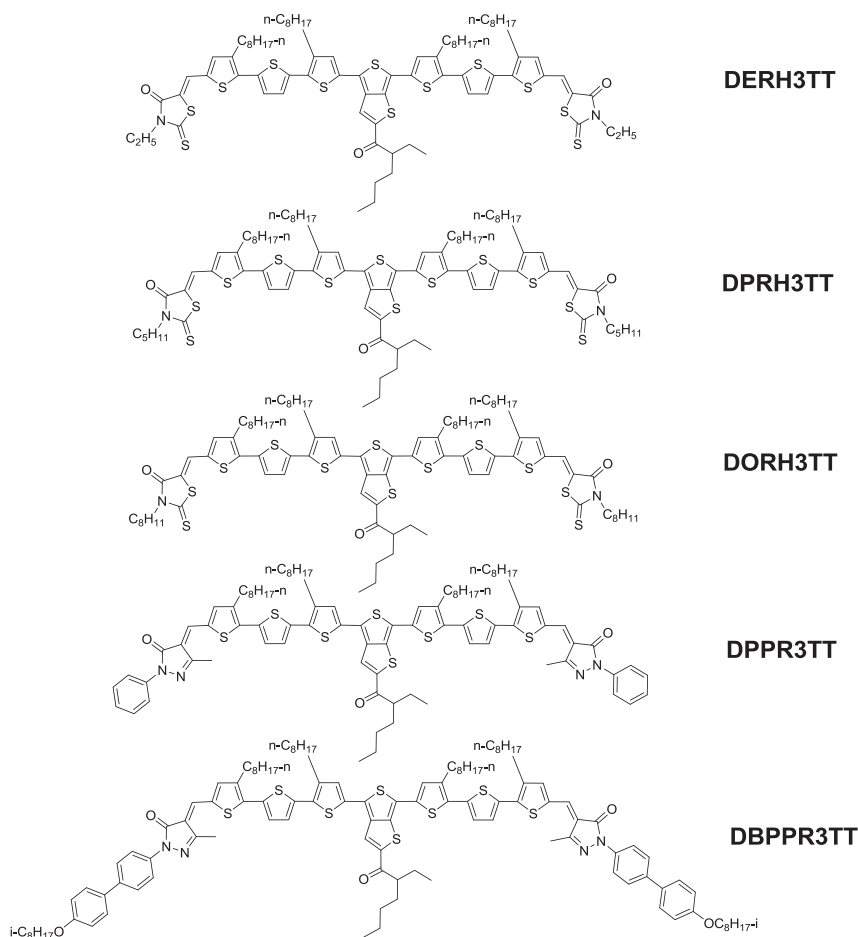


Chart 1. The chemical structures of DERH3TT, DPRH3TT, DORH3TT, DPPR3TT and DBPPR3TT.

absorption ability, to complete the A-D-A-D-A structure with its electron-drawing group. This was able to lower the band-gap of the molecules [11]. Moreover, different alkyl chains were introduced into the rhodanine and pyrazolone skeletons to tune their performances in the OPV devices. The thiophene and thienothiophene-one units were also modified with long alkyl chains to improve the solubility of the molecules in organic solvents, which ensured the formation of the photoactive layer for OPV devices. OPV cells with >3% efficiency was achieved under preliminarily optimized conditions.

2. Experimental section

2.1. Materials and methods

3-octylthiophene, NBS, Mg, BrCH₂CH₂Br, BrC₅H₁₁-n, BrC₈H₁₇-n and BuLi, were purchased from J&K Company. NiCl₂ (ppp), TsOH, glycol, Me₃SnCl, Pd(PPh₃)₄, pyridine, rhodanine, and 3-ethyl-rhodanin were purchased from Alfa Aesar Company. All solvents were dried and purified by standard methods prior to use. The procedure for synthesis of compounds 2, 5-dibromothiophene and 3-methyl-1-phenyl-2-pyrazolin-5-one were according to the literature [11]. The ¹H NMR and ¹³C NMR spectra were measured on a Bruker AC-400 and a Bruker AC-500 using TMS as internal standard. HRMS for small molecules (molecular weight <800) were recorded on a Fourier transform ion cyclotron resonance mass spectrometer (Bruker, APEX IV FTMS) with ESI resource. MS for macromolecules (molecular weight >800) were recorded on a

MALDI-TOF mass spectrometer (Bruker Daltonics Inc.). FTIR spectra were obtained on the instrument Bruker, TENSOR 27. Absorption spectra were observed with a JASCO V-570 spectrophotometer. Thermo-gravimetric and differential thermal analyses were carried out on Q50TGA instruments at an elevation temperature rate of 5 °C min⁻¹ under nitrogen flow. Cyclic voltammetry was performed with a computer controlled CHI600C electrochemical workstation using a conventional three electrode configuration consisting of a compartment electrolysis cell with a platinum button as a working electrode, platinum wire as a counter electrode, and Ag/AgCl reference electrode. Cyclic voltammograms were obtained in dichloromethane (1 × 10⁻³ M) using TBAPF₆ (0.1 M) as the supporting electrolyte at scan rate of 0.1 Vs⁻¹ with Fc/Fc⁺ as internal reference. Atomic force microscope (AFM) investigation was performed using SPA 400 in contact-mode and transmission electron microscopy (TEM) investigation was performed using JEM-2100F.

2.2. Synthesis

2.2.1. Synthesis of DCHO3TT

Compound **11** (1.70 g, 2.0 mmol), compound **5** (0.34 g, 0.8 mmol) and Pd(PPh₃)₄ (70 mg, 0.06 mmol) were added into dry toluene (100 mL) under protection of argon flow, and the mixture was refluxed under argon for 48 h under darkness. Then the toluene was removed and the crude black product was dissolved in CH₂Cl₂/THF (40/10 mL). Then HCl (4 M, 10 mL) was added and stirred at room temperature for 12 h. Subsequently, the mixture

was extracted by CH_2Cl_2 , dried by anhydrous Na_2SO_4 and purified by silica column with eluent as petroleum ether:AcOEt = 40:1 firstly, then petroleum ether: CH_2Cl_2 = 1:1. At last, red solid (0.81 g, 0.64 mmol) was obtained with two-step yield 64.1%, from compound **11** to DCHO3TT.

^1H NMR (400 MHz, CDCl_3): δ [ppm] = 9.85 (1H,s), 9.84 (1H,s), 7.87 (1H, s), 7.62 (1H, s), 7.61 (1H,s), 7.29 (1H, d, J = 4.0 Hz), 7.27 (1H, d, J = 4.0 Hz), 7.21 (1H, d, J = 4.0 Hz), 7.17 (1H, d, J = 4.0 Hz), 7.16 (1H, s), 7.12 (1H,s), 3.29–3.20 (1H, m), 2.87–2.80 (8H, m), 1.88–1.82 (2H, m), 1.78–1.66(8H, m), 1.43–1.25 (46H, m), 0.96–0.86 (18H, m). ^{13}C NMR (100 MHz, CDCl_3): δ [ppm] = 199.38, 182.47, 151.86, 142.57, 141.52, 141.50, 140.90, 140.66, 140.63, 140.58, 140.51, 140.40, 138.97, 138.96, 137.76, 137.72, 137.41, 136.36, 135.27, 134.86, 133.72, 133.65, 130.84, 129.95, 128.15, 127.90, 127.12, 127.09, 126.67, 126.38, 126.35, 122.18, 49.77, 34.72, 34.17, 32.35, 31.93, 31.91, 30.54, 30.36, 29.89, 29.74, 29.67, 29.66, 29.55, 29.49, 29.46, 29.32, 29.28, 26.00, 22.94, 22.72, 22.36, 14.12, 14.06, 13.98, 12.12. MS (MALDI-TOF) calcd. for $[\text{C}_{72}\text{H}_{94}\text{O}_3\text{S}_8]^+$: 1262.5; found: 1263.2.

2.2.2. Synthesis of DERH3TT

Compound DCHO3TT (0.12 g, 0.095 mmol) and excess 3-ethyl-rhodanin (0.12 g, 7.45 mmol) were dissolved in dry CHCl_3 (50 mL), followed by adding 3 drops pyridine. After being degassed for 5 times by argon, the mixture was refluxed for 48 h under argon and darkness. After remove of the solvent, the crude product was obtained. And then it was recrystallized in the mixture of CH_2Cl_2 and CH_3OH (Vol [CH_2Cl_2]/[CH_3OH] = 1:10) for 3 times, followed in the mixture of CH_2Cl_2 and hexane (Vol [CH_2Cl_2]/[hexane] = 1:20 for 3 times. Then obtained solid was further purified by Al_2O_3 column with eluent as petroleum ether: CH_2Cl_2 = 3:1 to get golden brown product (0.10 g, 0.064 mmol) with yield as 68.0%.

^1H NMR (400 MHz, CDCl_3): δ [ppm] = 7.86 (1H, s), 7.78 (1H, s), 7.77 (1H, s), 7.25 (1H, d, J = 3.2 Hz), 7.24–7.22 (3H, m), 7.19 (1H, d, J = 3.2 Hz), 7.16 (1H, d, J = 3.2 Hz), 7.14 (1H, s), 7.11 (1H, s), 4.20–4.18 (4H, m), 3.30–3.21(1H, m), 2.85–2.81 (8H, m), 1.90–1.82 (2H, m), 1.75–1.64 (8H, m), 1.45–1.26 (52H, m), 0.90–0.86 (18H, m). ^{13}C NMR (100 MHz, CDCl_3): δ [ppm] = 199.36, 192.07, 192.02, 167.32, 151.81, 142.54, 141.42, 141.37, 141.32, 141.21, 139.41, 139.13, 137.46, 137.28, 137.23, 137.08, 136.35, 135.50, 135.32, 135.26, 134.87, 133.65, 133.59, 130.92, 130.09, 128.10, 127.85, 127.36, 127.33, 127.03, 126.62, 126.33, 124.86, 124.78, 122.17, 121.59, 120.88, 120.70, 49.78, 39.96, 39.94, 32.35, 31.92, 31.89, 30.49, 30.31, 29.88, 29.76, 29.72, 29.66, 29.58, 29.52, 29.49, 29.45, 29.32, 29.29, 26.95, 25.99, 22.94, 22.70, 14.12, 13.99, 12.30, 12.12. MS (MALDI-TOF) calcd. for $[\text{C}_{82}\text{H}_{104}\text{N}_2\text{O}_3\text{S}_{12}]^+$: 1550.5; found: 1550.5. Melting point [$^\circ\text{C}$] = 215–226. FTIR (KBr): wavenumber [cm^{-1}] = 2953, 2920, 2849, 1693, 1657, 1570, 1456, 1412, 1383, 1345, 1319, 1235, 1127, 1101, 1080, 877, 816, 779, 732.

2.2.3. Synthesis of DPRH3TT

Compound DCHO3TT (0.20 g, 0.158 mmol), excess 3-pentyl-rhodanin (2.00 g, 9.85 mmol) and 3 drops pyridine were dissolved in dry CHCl_3 (70 mL). After it was degassed for 5 times with argon, the mixture continued to reflux for 48 h under argon and darkness. The solvent was removed and the crude product was recrystallized in mixture of CH_2Cl_2 and methanol (Vol [CH_2Cl_2 : MeOH] = 1:10) for 3 times and then in mixture of CH_2Cl_2 and hexane (Vol [CH_2Cl_2 : hexane] = 1:20) for 3 times. Then obtained solid was further purified by neutral Al_2O_3 column with eluent as petroleum ether: CH_2Cl_2 = 4:1 to get product (0.12 g, 0.11 mmol) with metal gloss with yield as 69.6%.

^1H NMR (400 MHz, CDCl_3): δ [ppm] = 7.83 (1H, s), 7.72 (1H, s), 7.70 (1H, s), 7.20–7.17 (4H, m), 7.13 (1H, d, J = 4.0 Hz), 7.10 (1H, d, J = 4.0 Hz), 7.06 (1H, s), 7.10 (1H, s), 4.10–4.04 (4H, m), 3.30–3.23

(1H, m), 2.83–2.75 (8H, m), 1.93–1.82 (2H, m), 1.71–1.69 (14H, m), 1.44–1.25 (52H, m), 0.94–0.87 (24H, m). ^{13}C NMR (100 MHz, CDCl_3): δ [ppm] = 199.27, 192.21, 192.17, 167.48, 151.71, 142.41, 141.24, 141.19, 141.17, 141.03, 139.44, 137.43, 137.21, 137.18, 137.06, 136.26, 135.41, 135.20, 135.19, 134.79, 133.54, 133.46, 130.94, 130.16, 127.96, 127.84, 127.18, 126.90, 126.40, 126.08, 124.72, 124.66, 122.18, 121.54, 120.74, 120.54, 49.77, 44.85, 32.32, 31.94, 31.91, 30.44, 30.28, 30.26, 29.89, 29.85, 29.73, 29.71, 29.59, 29.53, 29.49, 29.35, 29.31, 28.92, 26.69, 25.95, 22.96, 22.72, 22.28, 14.14, 14.13, 14.02, 13.93, 12.14. MS (MALDI-TOF) calcd. For $[\text{C}_{82}\text{H}_{116}\text{N}_2\text{O}_3\text{S}_{12}]^+$: 1634.6; found: 1634.8. Melting point [$^\circ\text{C}$] = 201–208. FTIR (KBr): wavenumber [cm^{-1}] = 2955, 2921, 2854, 1693, 1659, 1571, 1533, 1416, 1382, 1324, 1257, 1193, 1135, 1101, 1025, 777, 731.

2.2.4. Synthesis of DORH3TT

Compound DCHO3TT (0.20 g, 0.158 mmol), excess 3-octyl-rhodanin (2.00 g, 8.15 mmol) and 3 drops pyridine were dissolved in dry CHCl_3 (40 mL). After being degassed for 5 times with argon, the mixture was refluxed for 48 h under argon and darkness. Then the solvent was removed and the crude solid was obtained. It was recrystallized in mixture of CH_2Cl_2 and methanol (Vol [CH_2Cl_2 : MeOH] = 1:10) for 3 times and then in mixture of CH_2Cl_2 and hexane [CH_2Cl_2 : hexane = 1:20] for 3 times. At last, obtained solid was further purified by Al_2O_3 column (eluent as petroleum ether: CH_2Cl_2 = 6:1), to get product (0.19 g, 0.11 mmol) with metal gloss with yield as 69.9%.

^1H NMR (400 MHz, CDCl_3): δ [ppm] = 7.85 (1H, s), 7.74 (1H, s), 7.73 (1H, s), 7.20–7.19 (4H, m), 7.16 (1H, d, J = 3.6 Hz), 7.12 (1H, d, J = 3.6 Hz), 7.10 (1H, s), 7.06 (1H, s), 4.10–4.05 (4H, m), 3.30–3.23 (1H, m), 2.83–2.79 (8H, m), 1.92–1.84 (2H, m), 1.75–1.62 (14H, m), 1.48–1.22 (64H, m), 0.94–0.85 (24H, m). ^{13}C NMR (100 MHz, CDCl_3): δ [ppm] = 199.32, 192.25, 192.20, 167.51, 151.76, 142.48, 141.33, 141.28, 141.24, 141.12, 139.40, 139.12, 137.44, 137.22, 137.19, 137.06, 136.31, 135.48, 135.29, 135.24, 134.84, 133.60, 133.53, 130.93, 130.12, 128.05, 127.85, 127.27, 127.25, 126.97, 126.52, 126.21, 124.77, 124.70, 122.18, 121.57, 120.80, 120.61, 49.77, 44.88, 32.33, 31.93, 31.80, 30.47, 30.30, 30.29, 29.88, 29.80, 29.70, 29.68, 29.60, 29.55, 29.51, 29.47, 29.33, 29.30, 29.15, 27.01, 26.82, 25.97, 22.94, 22.71, 22.69, 22.65, 14.13, 14.11, 14.08, 14.00, 12.13. MS (MALDI-TOF) calcd. for $[\text{C}_{94}\text{H}_{128}\text{N}_2\text{O}_3\text{S}_{12}]^+$: 1718.8; found: 1719.6. Melting point [$^\circ\text{C}$] = 162–170. FTIR (KBr): wavenumber [cm^{-1}] = 2955, 2921, 2853, 1693, 1656, 1572, 1534, 1458, 1416, 1382, 1358, 1324, 1261, 1231, 1168, 1135, 1102, 1013, 812, 778, 727.

2.2.5. Synthesis of DPPR3TT

Compound DCHO3TT (0.10 g, 0.079 mmol), excess 1-phenyl-3-methyl-1H-pyrazol-5(4H)-one (1.00 g, 5.74 mmol) and 3 drops triethylamine were dissolved in dry CHCl_3 (50 mL). After it was degassed for 5 times with argon, the mixture was refluxed for 48 h under argon and darkness. Then the mixture was recrystallized in the mixture of CH_2Cl_2 and CH_3OH , (Vol [CH_2Cl_2 : CH_3OH] = 1:10) for 3 times, followed in the mixture of CH_2Cl_2 and hexane (Vol [CH_2Cl_2 : hexane] = 1:20) for 3 times. At last, the obtained solid was further purified by silica column (eluent as Vol [petroleum ether: CH_2Cl_2] = 4:1) to get product (0.051 g, 0.032 mmol) with yield as 40.9%.

^1H NMR (400 MHz, CDCl_3): δ [ppm] = 8.00 (4H, d, J = 6.4 Hz), 7.87 (1H, s), 7.79 (2H, d, J = 8.8 Hz), 7.46–7.39 (8H, m), 7.21–7.17 (4H, m), 7.14(1H, s), 7.11 (1H, s), 3.29–3.24 (1H, m), 2.89–2.82 (8H, m), 2.35 (3H, s), 2.34 (3H, s), 1.77–1.71 (8H, m), 1.34–1.26 (52H, m), 0.90–0.87 (18H, m). ^{13}C NMR (100 MHz, CDCl_3): δ [ppm] = 198.39, 161.47, 150.81, 148.82, 143.30, 143.09, 141.49, 141.08, 140.42, 139.97, 139.50, 137.56, 137.52, 137.11, 136.77, 136.72, 135.33, 134.48, 134.00, 133.25, 133.11, 132.64, 132.59, 127.78, 127.20, 127.13, 126.90, 126.02, 125.60, 125.58, 125.31, 123.70, 123.64, 121.18,

120.76, 120.62, 118.04, 118.02, 48.72, 31.36, 30.89, 29.43, 29.25, 28.84, 28.78, 28.69, 28.64, 28.60, 28.49, 28.46, 28.42, 28.30, 28.27, 25.00, 21.92, 21.67, 13.09, 12.96, 12.02, 11.09. MS (MALDI-TOF) calcd. for $[C_{92}H_{110}N_4O_3S_8]^+$: 1574.6; found: 1575.4. Melting point $[\text{°C}] = 153\text{--}165$. FTIR (KBr): wavenumber $[\text{cm}^{-1}] = 2956, 2924, 2849, 1728, 1677, 1658, 1588, 1555, 1499, 1457, 1397, 1368, 1299, 1177, 1139, 1093, 1023, 995, 785, 748$.

2.2.6. Synthesis of DBPPR3TT

Compound DCHO3TT (0.20 g, 0.152 mmol), excess compound 20 (2.00 g, 5.28 mmol) and 3 drops tri-ethylamine were dissolved in dry CHCl_3 (80 mL). After the mixture was degassed for 5 times with argon, it was refluxed for 48 h under argon and darkness. Then the mixture was recrystallized in the mixture of CH_2Cl_2 and CH_3OH (Vol $[\text{CH}_2\text{Cl}_2 : \text{MeOH}] = 1:10$) for 3 times, followed in the mixture of CH_2Cl_2 : hexane (Vol $[\text{CH}_2\text{Cl}_2 : \text{hexane}] = 1:20$) for 3 times. The obtained solid was further purified by silica column (eluent as Vol [petroleum ether: CH_2Cl_2] = 4:1) to get product (0.102 g, 0.051 mmol) with yield as 33.6%.

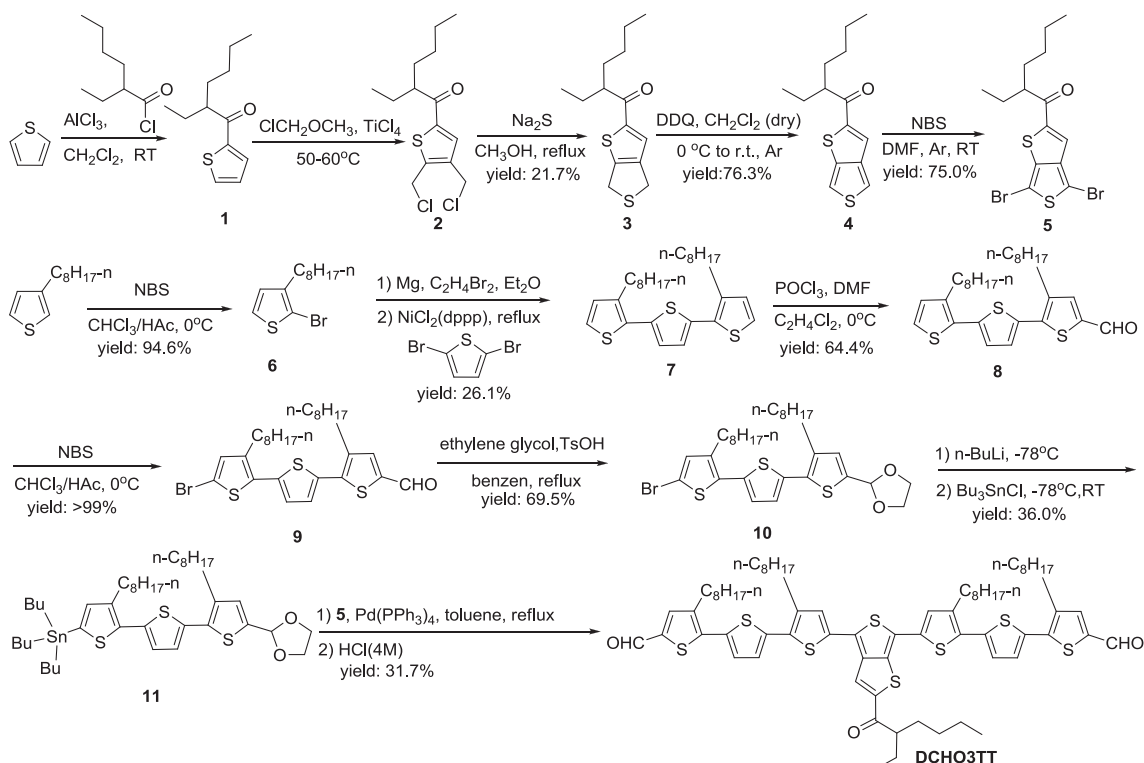
^1H NMR (400 MHz, CDCl_3): δ [ppm] = 8.04 (4H, d, $J = 8.4$ Hz), 7.88 (1H, s), 7.81 (1H, s), 7.19 (1H, s), 7.61 (4H, d, $J = 8.8$ Hz), 7.54 (4H, d, $J = 8.4$ Hz), 7.48 (1H, s), 7.47 (1H, s), 7.43 (1H, d, $J = 4.0$ Hz), 7.42 (1H, d, $J = 4.0$ Hz), 7.22 (1H, d, $J = 4.0$ Hz), 7.20 (1H, d, $J = 4.0$ Hz), 7.16 (1H, s), 7.12 (1H, s), 6.98 (4H, d, $J = 8.8$ Hz), 3.88–3.89 (4H, m), 3.30–3.23 (1H, m), 2.91–2.82 (8H, m), 2.37 (3H, s), 2.36 (3H, s), 1.91–1.82 (2H, m), 1.78–1.72 (8H, m), 1.35–1.25 (67H, m), 1.90–0.84 (35H, m). ^{13}C NMR (100 MHz, CDCl_3): δ [ppm] = 199.43, 162.47, 158.93, 158.91, 149.94, 145.04, 144.66, 144.61, 144.34, 144.11, 142.56, 141.50, 141.48, 140.58, 138.14, 137.75, 137.31, 137.26, 137.24, 137.18, 135.50, 135.45, 135.07, 134.33, 133.70, 133.67, 133.65, 133.12, 133.08, 128.28, 128.20, 127.89, 127.09, 127.08, 126.96, 126.66, 126.39, 121.84, 121.71, 119.25, 114.87, 70.69, 53.40, 41.38, 39.47, 36.09, 35.69, 34.70,

34.54, 32.40, 31.92, 31.60, 30.60, 30.48, 30.30, 29.88, 29.80, 29.71, 29.67, 29.66, 29.63, 29.51, 29.45, 29.32, 29.14, 29.08, 26.95, 25.31, 23.94, 23.09, 22.95, 22.70, 22.67, 22.63, 14.12, 13.99, 13.07, 12.12, 11.42, 11.14. MS (MALDI-TOF) calcd. for $[C_{120}H_{150}N_4O_5S_8]^+$: 1985.0; found: 1984.2. Melting point $[\text{°C}] = 205\text{--}212$. FTIR (KBr): wavenumber $[\text{cm}^{-1}] = 2957, 2919, 2848, 1721, 1681, 1656, 1595, 1497, 1464, 1388, 1361, 1296, 1263, 1241, 1175, 1138, 1029, 996, 816, 794, 729$.

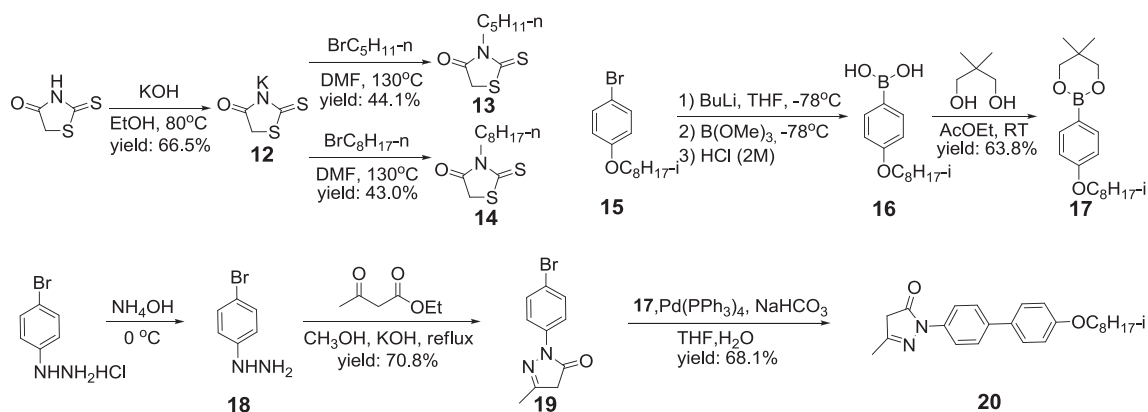
3. Results and discussion

3.1. Material synthesis and characterization

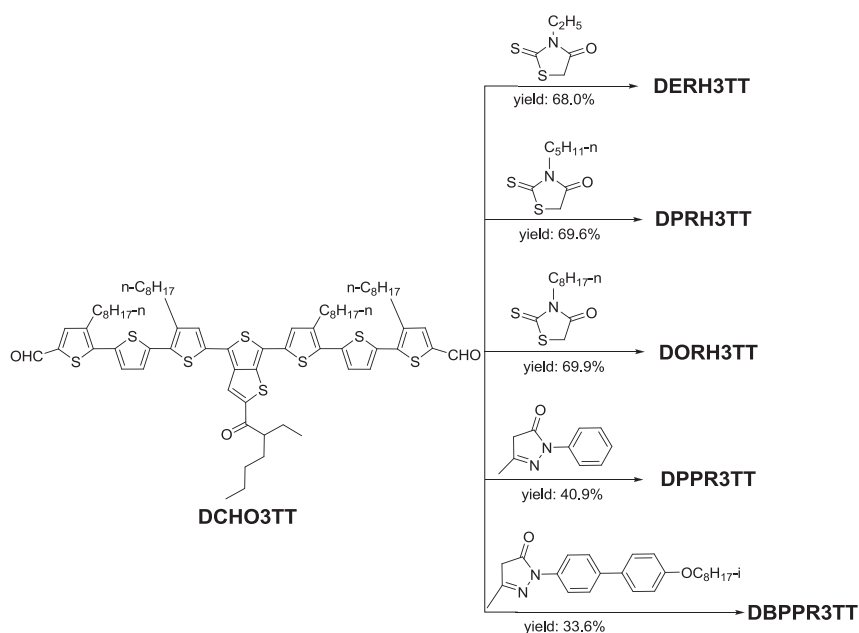
The synthetic methods are outlined in Schemes 1–3. 1-(4,6-dibromothieno[3,4-b]thiophen-2-yl)-2-ethylhexan-1-one (**3**) and 5-bromo-3,3-dioctyl-2,2',2'''-terthiophene-2-carbaldehyde (**9**) were synthesized according to the reported procedures, respectively [11,28]. It is noteworthy to mention that the synthesis of compound **4** was optimized by using 2,3-dichloro-5,6-dicyano-1,4-benzoquinone (DDQ) instead of *m*-chloroperoxybenzoic acid to oxidize compound **3** to form the aromatic thiophene ring [28]. This one-step method we proposed in the present work significantly simplified the synthesis process with improved yields of the target compound. Due to their active reactions with BuLi, the aldehyde-groups of compound **9** were first protected with glycol to form a five-ring diether for the synthesis of 5-(1,3-dioxolan-2-yl)-3,3-dioctyl-2,2',2'''-terthiophene-2-tributylstannane (**11**) [29]. The protective groups can be easily removed under acidic condition after the Stille-coupling reaction. The reaction of precursor DCHO3TT (see Scheme 3), catalyzed by piperidine, with 3-ethyl-rhodanin produced DERH3TT compound in a yield of 68.0%. DPRH3TT and DORH3TT were then synthesized with 3-pentyl-rhodanin and 3-octyl-rhodanin as terminal



Scheme 1. Synthetic routes for the monomers and precursor DCHO3TT of the target molecules.



Scheme 2. Synthetic routes for the terminal groups 13, 14 and 20.



Scheme 3. Synthetic routes for the target molecules under the condition: peridine (3 drops), CHCl_3 , Ar, darkness, reflux.

groups in similar yields [30]. Both DPRH3TT and DORH3TT showed high solubility in organic solvents including CHCl_3 , CH_2Cl_2 and *o*-dichlorobenzene (ODCB). The molecular energy level, absorption ability and hole-mobility of the synthesized A-D-A-D-A small molecules were tuned by using pyrazolone derivatives as the terminal groups. The yields of the pyrazolone terminated DPPR3TT and DBPPR3TT are in the range of 30–40%, slightly lower than those of the rhodanin derivatives terminated small molecules. This can be attributed to the high hindrance of the pyrazolone groups.

The performance of the A-D-A-D-A small molecule based photovoltaic device is highly dependent on the solubility, film-forming property and stability of the small molecule. The solubility of DERH3TT, DPPR3TT and DBPPR3TT is 10 mg mL^{-1} in CHCl_3 and those of DPRH3TT and DORH3TT in CHCl_3 are 15 mg mL^{-1} and 20 mg mL^{-1} , respectively. The decomposition temperatures of DERH3TT, DPRH3TT, DORH3TT, DPPR3TT and DBPPR3TT are 395, 393, 394, 314 and 322 °C, respectively

(Fig. 1). Therefore, these compounds can be applied in the optoelectronic devices at the annealing temperatures between 100 and 200 °C. DSC analysis under nitrogen atmosphere from 20 to 250 °C indicates no obvious glass transition occurred in these compounds. The rhodanin derivatives terminated DERH3TT, DPRH3TT and DORH3TT displayed obvious melting temperatures. The melting temperature (T_m) of DORH3TT is 167 °C, which is 39 °C or 56 °C lower than those of DERH3TT and DPRH3TT, respectively, indicating that the octyl-terminal chains can affect the melting temperature of the compounds. The pyrazolone derivatives terminated DPPR3TT and DBPPR3TT showed no obvious melting temperature below their decomposition temperatures.

3.2. XRD characterization and electrochemical properties

The packing of the molecules in the solid state was characterized with X-ray powder diffraction (XRD) [31]. As shown

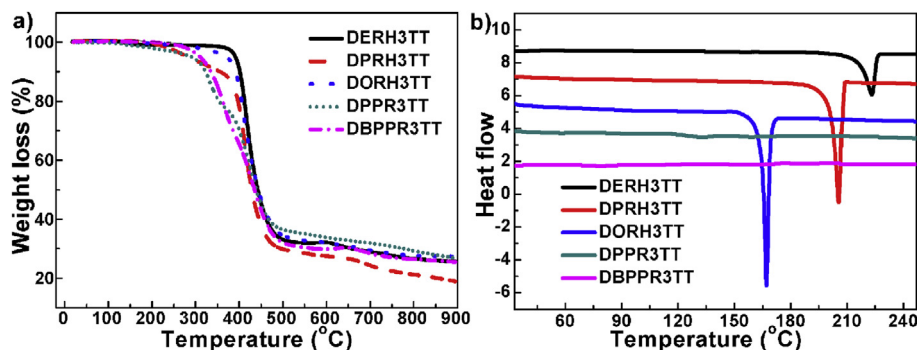


Fig. 1. a) TGA plots of DERH3TT, DPRH3TT, DORH3TT, DPPR3TT and DBPPR3TT obtained at a heating rate of $10\text{ }^{\circ}\text{C min}^{-1}$ under N_2 atmosphere; b) DSC curves of the small molecule compounds obtained under N_2 flow at a heating rate of $10\text{ }^{\circ}\text{C min}^{-1}$.

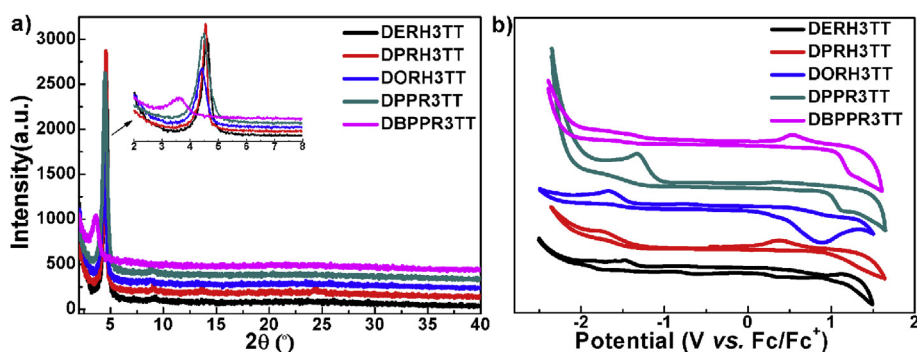


Fig. 2. a) Powder XRD patterns of the small molecule films; b) cyclic voltammograms of the five compounds.

in Fig. 2a, DERH3TT, DPRH3TT, DORH3TT, DPPR3TT and DBPPR3TT exhibited diffraction peaks at 2θ of 4.61° , 4.56° , 4.42° , 4.49° and 3.66° , respectively, corresponding to the backbone distances of 19.15, 19.35, 19.97, 19.67 and 24.10 Å, respectively. This indicates that the long terminal alkyl chain and big biphenyl terminal groups can prevent the molecules from approaching.

Fig. 2b shows the CV curves of DERH3TT, DPRH3TT, DORH3TT, DPPR3TT and DBPPR3TT, which can be used to determine their HOMO energy levels. Their onset oxidation potentials are 0.19 V, 0.15 V, 0.21 V, 0.35 V and 0.34 V, respectively. Their HOMO levels were calculated with $E_{\text{HOMO}} = -(E_{\text{ox}} + 4.80)$ as -4.99 , -4.95 , -5.01 , -5.15 and -5.14 eV, respectively [32]. Pyrazolone derivatives terminated DPPR3TT and DBPPR3TT exhibited

lower HOMO levels than the rhodanin derivatives terminated DERH3TT, DPRH3TT and DORH3TT.

3.3. Photophysical properties

Fig. 3 shows the UV–Vis absorption spectra of the five synthesized A-D-A-D-A compounds in solution and film. Due to the thienothiophene-one π -bridges of the A-D-A-D-A structures, all five compounds exhibited a strong absorption band ranging from 250 to 700 nm in chloroform (Fig. 3a). When rhodanin or pyrazolone derivatives were introduced onto the terminal of the precursor DCHO3TT, its absorption coefficient was significantly enhanced and the absorption peaks was red-shifted about 25–30 nm in solution. This indicates that the electron-withdrawing

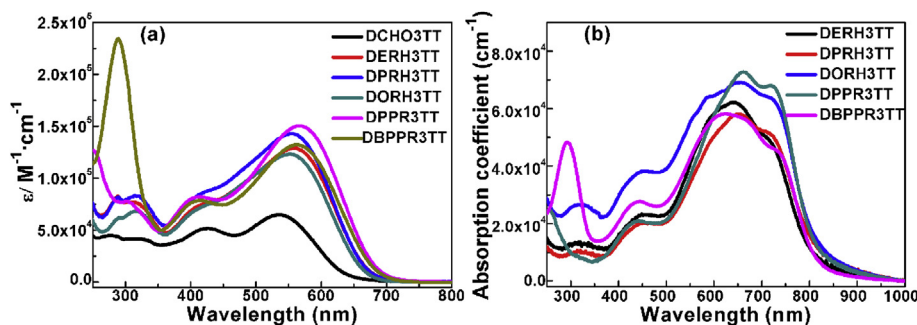


Fig. 3. (a) UV–Vis absorption spectra of the compounds in chloroform; (b) UV–Vis absorption spectra of the compound films.

Table 1
Electrochemical and optical properties and hole mobility of the compounds.

Small molecules	λ_{max}	λ_{max}	$E_{\text{g,opt}}^{\text{a}}$ (eV)	HOMO ^b (eV)	LUMO ^b (eV)	μ^{c} ($\text{cm}^2 \text{V}^{-1} \text{s}^{-1}$)
	(nm)	(nm)				
	Solution					
	Film					
DERH3TT	559	642	1.54	-4.99	-3.45	8.51×10^{-4}
DPRH3TT	556	652	1.52	-4.95	-3.43	5.04×10^{-4}
DORH3TT	554	657	1.52	-5.01	-3.49	1.12×10^{-4}
DPPR3TT	567	662	1.52	-5.15	-3.63	2.38×10^{-3}
DBPPR3TT	562	630	1.52	-5.14	-3.62	5.33×10^{-4}

^a Calculated from the absorption band edge of these compounds, $E_{\text{g,opt}} = 1240/\lambda_{\text{edge}}$.

^b Calculated by the equation $E_{\text{LUMO}} = E_{\text{HOMO}} + E_{\text{g,opt}}$ [29].

^c Hole Mobility of these molecular films were measured by field effect transistors [28].

groups can increase the light absorption of the small molecules. Interestingly, compared with rhodanine-terminal derivatives, the pyrazolone-terminal derivatives showed ~5 nm red-shifts absorption peak. This may be attributed to the stronger electron-drawing property of pyrazolone derivatives. As expected, extending the conjugated terminal group increased the absorption intensity in UV region (Fig. 3a).

Compared with those of their solutions, the absorption bands of DERH3TT, DPRH3TT, DORH3TT, DPPR3TT and DBPPR3TT films are stronger, broader and red-shifted by ca. 100 nm (Fig. 3b). In addition, a new vibronic peak at ca. 715 nm, close to absorption edge, was observed, indicating the ordered structure and strong π - π stacking interaction between the molecular backbones at solid status. The absorption edges of DERH3TT, DPRH3TT, DORH3TT,

DPPR3TT and DBPPR3TT films are at ca. 807, 817, 815, 812 and 814 nm, corresponding to the optical band gaps ($E_{\text{g,opt}}$) of 1.54, 1.52, 1.52, 1.52, and 1.52 eV, respectively (Table 1). These results indicate that the small molecules are good light absorbers and possess compatible energy levels to the acceptor PCBM.

3.4. Hole mobility of the target molecular films

Compatible hole mobility to PCBM is usually required for donors to achieve the balanced electron and hole mobility of the small molecules and PCBM blends, which is very crucial for the high performance solar cells. To measure the carrier mobility of the compounds, bottom-gate and bottom-contact field effect transistors (FETs) were fabricated [31]. The source-drain electrodes with 8 nm Cr and 60 nm Au layers were prepared by thermal evaporation with p-doped Si/300 nm SiO₂ as a substrate. The thin small molecule films were spin-coated on the electrodes with their chloroform solutions (5 mg mL⁻¹) at 1700 rpm for 1 min Fig. 4 shows the transfer characteristic curve of DERH3TT device. The characteristic curves of the devices prepared with other A-D-A-D-A small molecules compounds can be found in the Supporting Information (Fig. S19). The hole mobility (μ) of the solar cell device was calculated with the equation $I_{\text{DS}} = (W/2L) \cdot \mu \cdot C_i \cdot (V_G - V_T)^2$, where I_{DS} , W , L , C_i , V_G and V_T were the source-drain current, the channel width, the channel length, the gate dielectric capacitance per unit area (SiO₂, 300 nm, $C_i = 11 \text{ nF cm}^{-2}$), the gate voltage and threshold voltage, respectively. The results indicate that DERH3TT, DPRH3TT, DORH3TT, DPPR3TT and DBPPR3TT have a hole-mobility of 8.51×10^{-4} , 5.04×10^{-4} , 1.12×10^{-4} , 2.38×10^{-3} and $5.33 \times 10^{-4} \text{ cm}^2 \text{V}^{-1} \text{s}^{-1}$, respectively, in the saturated regime, which are consistent with that of P3HT [33] and the previous report [11]. These results indicate that shorter alkyl terminal chain is favorable for hole-mobility and the phenyl-pyrazolone terminal groups increase the hole-mobility of the molecule.

3.5. Theoretical computations

To further understand the structure and physicochemical properties of the compounds, the molecular geometries and electronic wave functions of frontier orbital were investigated with theoretical computation. Since the computations of both geometry optimizations and excited-state were conducted on their chloroform solutions, the solvent effects were included in the framework of the polarizable continuum model (PCM). The detailed computation is described in the Supporting Information. Due to the slight effects of the long side alkyl chain on the energy level of the whole molecule, n-octyl groups on the thiophene were simplified as the methyl groups in the model [34]. Fig. 5 shows the theoretical electronic wave functions of HOMO and LUMO of DERH3TT, DPRH3TT, DORH3TT, DPPR3TT and DBPPR3TT. The electronic wave functions of the frontier orbital were delocalized on the whole main chain. Relatively high HOMO densities were observed on the central thienothiophene-one group and high LUMO densities were found on the terminal rhodanine or pyrazolone groups, which were consistent with the previous reports [11,16]. Furthermore, the increase of the alkyl chain on N-rhodanine and the substitutions of N-pyrazolone showed almost no effect on the HOMO and LUMO of the compounds (Table 2). Theoretically, the less hindrance around the electron-withdrawing terminal groups such as in DERH3TT would be favorable for the electron transfer from the donor molecules to the fullerene acceptors in the bulk hetero-junction OPV [16]. In all, the theoretical computation results are in good agreement with experimental results (Table 1).

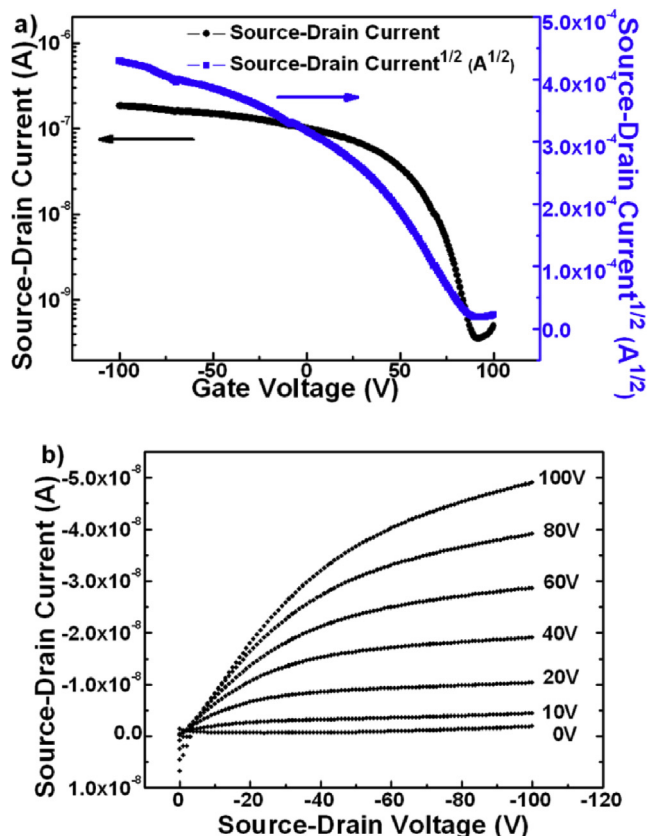
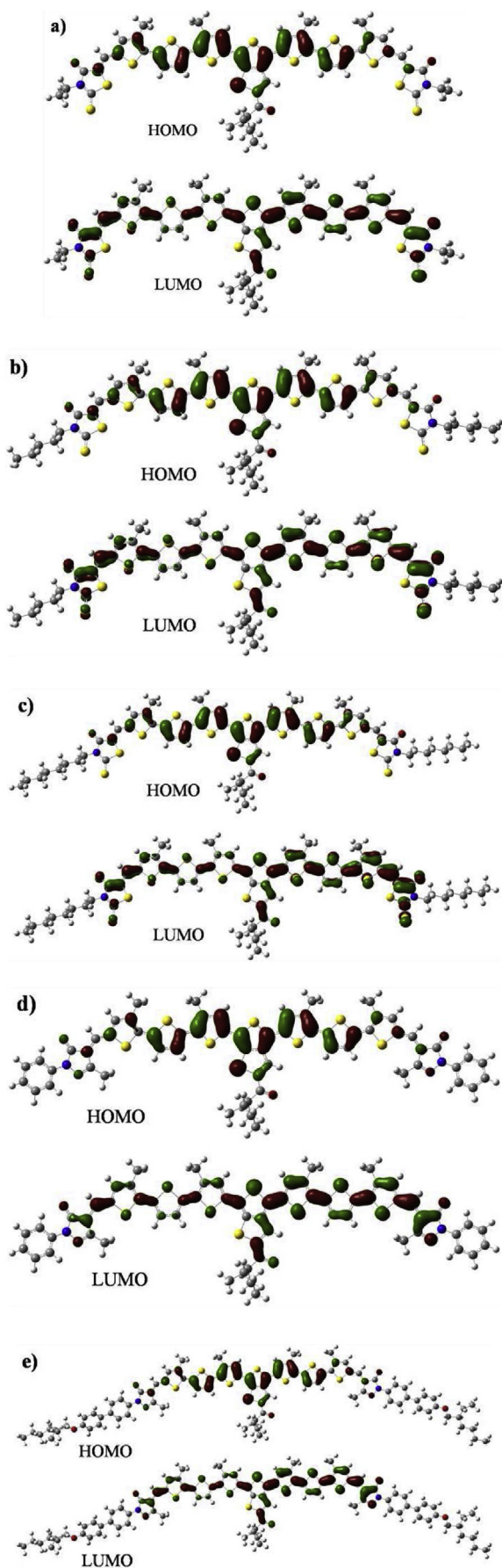


Fig. 4. a) Transfer and b) output characteristics of the DERH3TT solar cell device.

**Table 2**

B3LYP/6-31G* calculated HOMO and LUMO energies, excitation energies and oscillator strengths of the lowest singlet excited states (S1). (Energies are in unit of eV).

Small molecules	HOMO (eV)	LUMO (eV)	E(S1) (eV)	Oscillator (S1)
DERH3TT	-4.85	-3.00	1.55	3.00
DPRH3TT	-4.86	-2.99	1.57	2.97
DORH3TT	-4.85	-2.99	1.57	3.02
DPPR3TT	-4.91	-3.05	1.57	3.21
DBPPR3TT	-4.92	-3.04	1.58	3.34

3.6. Applications of the A-D-A-D-A small molecule compounds in solar cells

To determine the photovoltaic properties of these compounds, bulk-heterojunction OSCs were fabricated with them as the donor and PC₇₀BM as the acceptor in the ITO/PEDOT:PSS/photoactive layer/PFN/Al device. The photoactive layer was prepared by the conventional spin-coating with the chloroform solutions of the compounds. The best *J*-*V* curves of the devices are shown in Fig. 6a and the corresponding photovoltaic performance is summarized in Table 3. Since the solubility of DERH3TT, DPPR3TT and DBPPR3TT in chloroform is ~10 mg mL⁻¹, their solutions with concentrations of 10 and 8 mg mL⁻¹ were used for the preparation of the photoactive layer (Table S1 and S2). The DERH3TT device prepared with a D/A weight ratio of 1:0.8 at a donor concentration of 10 mg mL⁻¹ showed the best photovoltaic performance with a high open circuit voltage (*V*_{oc}) of 0.81 V, a short-circuit current density (*J*_{sc}) of 7.51 mA cm⁻², a fill factor (*FF*) of 52.8%, and a power conversion efficiency (*PCE*) of 3.19%.

In view of the high solubility of DPPR3TT and DOPPR3TT in chloroform, respectively, therefore, higher concentrations of the donors were used for the fabrication of their solar cells. As shown in Table 3 and S3, the *PCE* of the devices prepared with 12 mg mL⁻¹ donor solutions dramatically dropped due to the decreased *J*_{sc}. It can be explained that the thickness of the active layer is increased with the increase of the donor concentration under the same film-formation condition, which increased the recombination probability of the excitation, leading to lower *J*_{sc}.

The external quantum efficiency (*EQE*) spectra of the optimized DERH3TT, DPRH3TT, DORH3TT, DPPR3TT and DBPPR3TT devices are shown in Fig. 6b. The DERH3TT/PC₇₁BM device exhibited high photo conversion efficiency in the wavelength range from 300 to 800 nm, with a highest *EQE* value of 38% at 430 nm. The theoretical *J*_{sc} of DERH3TT integrated from *EQE* spectrum is 7.25 mAcm⁻² and has about 5% deviation from the experimental result. Although the *PCE*s of the A-D-A-D-A small molecule solar cells are relatively low, their efficient photo conversion efficiency ranges are broader than those of the similar small molecule devices previously reported [11–13]. In addition, despite the similar absorption spectra, band-gap and hole-mobility of the compounds, the DPPR3TT and DBPPR3TT devices showed lower *EQE*s and higher *J*_{sc} than the DERH3TT, DPRH3TT and DORH3TT devices. This can be explained that DPPR3TT and DBPPR3TT compounds can not form a good phase separation with PC₇₁BM as shown in the AFM and TEM images of the their blends with PC₇₁BM (Fig. S21 and S22).

Fig. 5. The electronic wave functions of the lowest unoccupied (LUMO) and the highest occupied (HOMO) in the DERH3TT (a), DPRH3TT (b), DORH3TT (c), DPPR3TT (d) and DBPPR3TT (e) chloroform solutions, depicted at isodensity surface of 0.025 au and calculated at B3LYP/6-31G* level.

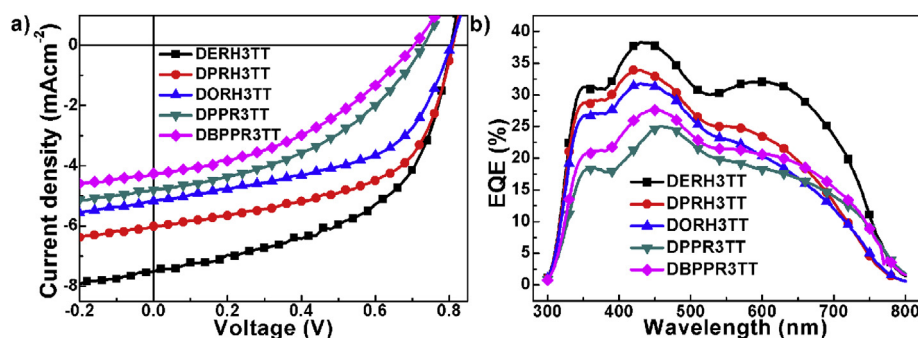


Fig. 6. (a) J – V curves of the solar cells with the photoactive layer composed of DERH3TT, DPRH3TT, DORH3TT, DPPR3TT and DBPPR3TT/PC₇₁BM (1:0.8, w/w) without additives and annealing treatment; (b) EQE plots of the solar cells with an active layer composed of DERH3TT, DPRH3TT, DORH3TT, DPPR3TT and DBPPR3TT/PC₇₁BM (1:0.8, w/w).

Table 3

Device performance parameters for BHJ solar cells based on DERH3TT, DPRH3TT, DORH3TT, DPPR3TT and DBPPR3TT with donor concentration of 10 mg mL⁻¹.

Donor molecular	D/A ratio	D (mg mL ⁻¹)	V _{oc} (V)	J _{sc} (mA cm ⁻²)	FF (%)	PCE (%)
DERH3TT	1:0.5	10	0.82	6.72	50.8	2.80
	1:0.8	10	0.81	7.51	52.8	3.19
	1:1	10	0.77	5.92	30.4	1.39
DPRH3TT	1:0.8	10	0.81	6.01	55.9	2.72
	1:0.8	10	0.79	5.28	52.3	2.19
DORH3TT	1:0.8 ^a	10	0.82	6.03	50.3	2.49
	1:0.8	10	0.73	4.80	42.3	1.48
DBPPR3TT	1:0.8	10	0.71	4.26	40.0	1.21

^a devices were annealed at 160 °C.

3.7. Morphologies of the A-D-A-D-A small molecule photoactive layers

The surface morphologies of DERH3TT/PC₇₁BM, DPRH3TT/PC₇₁BM, DORH3TT/PC₇₁BM, DPPR3TT/PC₇₁BM and DBPPR3TT/PC₇₁BM (1:0.8, w/w) blend films spin-coated from their chloroform solutions were imaged with AFM. Their average roughness are 4.63, 4.90, 7.42, 25.3, 29.4 nm, respectively, indicating that the DERH3TT, DPRH3TT and DORH3TT with alkyl chain terminal groups have better miscibility with PC₇₁BM molecules in the blend film than DPPR3TT and DBPPR3TT with large phenyl groups.

Fig. 7 shows the TEM images of the A-D-A-D-A small molecule photoactive layers of the solar cell devices. As shown in Fig. 7a and b, DERH3TT and DPRH3TT are continuous interpenetrating networks with the domain sizes more than 100 nm. Blending PC₇₁BM with DORH3TT distributed the domains with an obvious aggregation, resulting in an irregular morphology (Fig. 7c). The blending of PC₇₁BM with DPPR3TT and DBPPR3TT even broke their continuous interpenetrating networks, leading to low efficient excitation dissociation, charge transport, and thus lower J_{sc}. Therefore, the dissatisfactory solar cell performance is at least in some degree attributed to irregular morphology of the blend film of the compounds with PC₇₁BM and fine design of the A-D-A-D-A small molecule structure is critical to obtain desired solar cell performances.

4. Conclusions

In summary, DERH3TT, DPRH3TT, DORH3TT, DPPR3TT and DBPPR3TT molecules with the A-D-A-D-A structure and thienothiophene-one as the central building block have been designed, synthesized and well characterized. They showed broad UV–Vis absorption spectrum, high molar absorption coefficient and good solubility in most organic solvents. In addition, they have

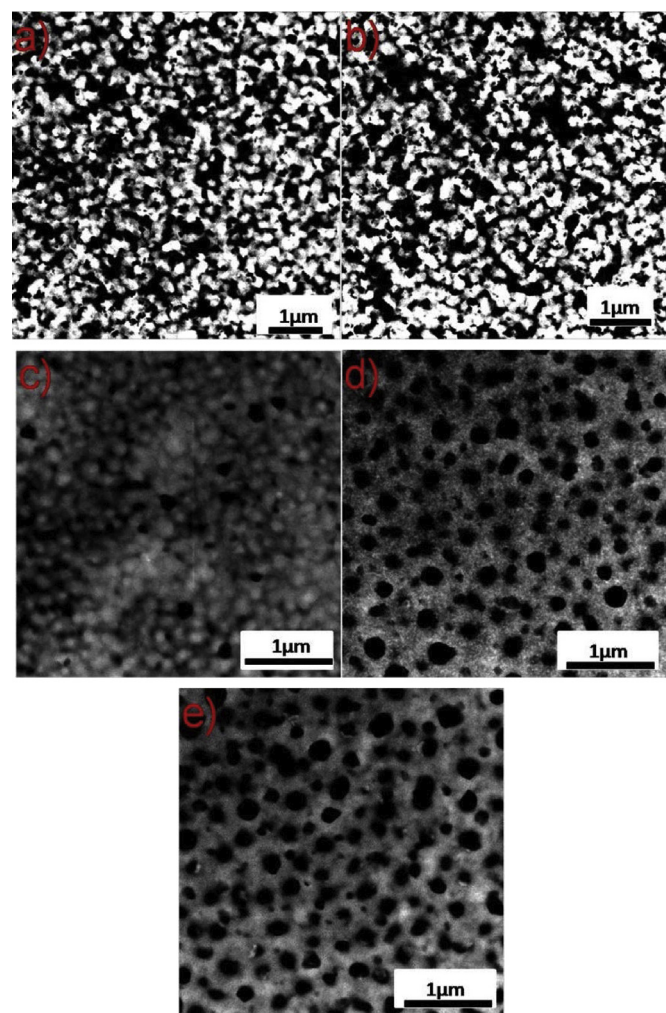


Fig. 7. TEM images of DERH3TT (a), DPRH3TT (b), DORH3TT (c), DPPR3TT (d) and DBPPR3TT (e)/PC₇₁BM (1:0.8, w/w) photoactive layers.

high hole-mobility and compatible energy level with PCBM, as well as good photoelectric response in the range from 300 to 800 nm. The solar cell device prepared with the short-alkyl-chain terminated DERH3TT as the photoactive layers showed a highest J_{sc} and a highest PCE of 3.19%. The high molar absorption coefficient, broad photoelectric response range and the high hole-mobility of these compounds make them the promising candidates for the high efficiency solution processed organic photovoltaic cells.

Acknowledgments

The authors gratefully acknowledge the financial support from the National Basic Research Program (2011CB933303) and the National Natural Science Foundation of China (NSFC) (21321001, 21371012).

Appendix A. Supplementary data

Supplementary data related to this article can be found at <http://dx.doi.org/10.1016/j.dyepig.2015.05.009>.

References

- [1] Leung M, Chang C, Wu M, Chuang K, Lee J, Shieh S, et al. 6-N,N-Diphenylaminobenzofuran-derived pyran containing fluorescent dyes: a new class of high-brightness red-light-emitting dopants for OLED. *Org Lett* 2006;8(12):2623–6.
- [2] Wei Y, Chen C. Doubly ortho-linked cis-4,4'-bis(diarylamino)stilbene/fluorene hybrids as efficient nondoped, sky-blue fluorescent materials for optoelectronic applications. *J Am Chem Soc* 2007;129(24):7478–9.
- [3] Yao Y, Xiao J, Wang X, Deng Z, Zhang B. Starburst DCM-type red-light-emitting materials for electroluminescence applications. *Adv Funct Mater* 2006;16(5):709–18.
- [4] Xiao J, Yang B, Wong J, Liu Y, Wei F, Tan K, et al. Synthesis, characterization, self-assembly, and physical properties of 11-methylbenzo[d]pyreno[4,5-b]furan. *Org Lett* 2011;13(12):3004–7.
- [5] Xiao J, Liu S, Liu Y, Ji L, Liu X, Zhang H, et al. Synthesis, structure, and physical properties of 5,7,14,16-tetraphenyl-8,9,12:13-bisbenzo-hexatwistacene. *Chem Asian J* 2012;7(3):561–4.
- [6] Komori T, Nakanotani H, Yasuda T, Adachi C. Light-emitting organic field-effect transistors based on highly luminescent single crystals of thiophene/phenylene co-oligomers. *J Mater Chem C* 2014;2(25):4918–21.
- [7] Wang C, Zhang J, Long G, Aratani N, Yamada H, Zhao Y, et al. Synthesis, structure, and air-stable N-type field-effect transistor behaviors of functionalized octaazanonacene-8,19-dione. *Angew Chem Int Ed* 2015. <http://dx.doi.org/10.1002/anie.201500972>.
- [8] Walker B, Tamayo AB, Dang X, Zalar P, Seo J, Garcia A, et al. Nanoscale phase separation and high photovoltaic efficiency in solution-processed, small-molecule bulk heterojunction solar cells. *Adv Funct Mater* 2009;19(19):3063–9.
- [9] Liu Y, Wan X, Wang F, Zhou J, Long G, Tian J, et al. High-performance solar cells using a solution-processed small molecule containing benzodithiophene unit. *Adv Mater* 2011;23(45):5387–91.
- [10] Cho N, Song K, Lee J, Ko J. Facile synthesis of fluorine-substituted benzothiadiazole-based organic semiconductors and their use in solution-processed small-molecule organic solar cells. *Chem Eur J* 2012;18(36):11433–9.
- [11] Li Z, He G, Wan X, Liu Y, Zhou J, Long G, et al. Solution processable rhodanine-based small molecule organic photovoltaic cells with a power conversion efficiency of 6.1%. *Adv Energy Mater* 2012;2(1):74–7.
- [12] He G, Li Z, Wan X, Liu Y, Zhou J, Long G, et al. Impact of dye end groups on acceptor–donor–acceptor type molecules for solution-processed photovoltaic cells. *J Mater Chem* 2012;22(18):9173–80.
- [13] Chen W, Yang X, Long G, Wan X, Chen Y, Zhang Q. A perylene diimide (PDI)-based small molecule with tetrahedral configuration as a non-fullerene acceptor for organic solar cells. *J Mater Chem C* 2015. <http://dx.doi.org/10.1039/C5TC00865D>.
- [14] Sharenko A, Proctor CM, van der Poll TS, Henson ZB, Nguyen T, Bazan GC. A high-performing solution-processed small molecule: perylene diimide bulk heterojunction solar cell. *Adv Mater* 2013;25(32):4403–6.
- [15] Liu Y, Yang Y, Chen C, Chen Q, Dou L, Hong Z, et al. Solution-processed small molecules using different electron linkers for high-performance solar cells. *Adv Mater* 2013;25(33):4657–62.
- [16] Shen S, Jiang P, He C, Zhang J, Shen P, Zhang Y, et al. Solution-processable organic molecule photovoltaic materials with bithienyl-benzodithiophene central unit and indenone end groups. *Chem Mater* 2013;25(11):2274–81.
- [17] Zhou J, Zuo Y, Wan X, Long G, Zhang Q, Ni W, et al. Solution-processed and high-performance organic solar cells using small molecules with a benzodithiophene unit. *J Am Chem Soc* 2013;135(23):8484–7.
- [18] Chen Y, Wan X, Long G. High performance photovoltaic applications using solution-processed small molecules. *Acc Chem Res* 2013;46(11):2645–55.
- [19] Bredas J. When electrons leave holes in organic solar cells. *Science* 2014;343(6170):492–3.
- [20] Kim Y, Baek J, Ha J, Chung DS, Kwon S, Park C, et al. A high-performance solution-processed small molecule: alkylselenophene-substituted benzodithiophene organic solar cell. *J Mater Chem C* 2014;2(24):4879–92.
- [21] Löbert M, Mishra A, Uhrich C, Pfeiffer M, Bäuerle P. Synthesis and characterization of benzo- and naphtho[2,1-b:3,4-b']dithiophene-containing oligomers for photovoltaic applications. *J Mater Chem C* 2014;2(24):4879–92.
- [22] Sun Y, Welch G, Leong W, Takacs CJ, Bazan GC, Heeger AJ. Solution-processed small-molecule solar cells with 6.7% efficiency. *Nat Mater* 2012;11(1):44–8.
- [23] Li G, Zhao Y, Li J, Cao J, Zhu J, Sun X, et al. Synthesis, characterization, physical properties, and OLED application of single BN-fused perylene diimide. *J Org Chem* 2015;80(1):196–203.
- [24] Zhang Q, Xiao J, Yin Z, Duong HM, Qiao F, Boey F, et al. Synthesis, characterization, and physical properties of a conjugated heteroacene: 2-methyl-1,4,6,7,8,9-hexaphenylbenz(g)isoquinolin-3(2H)-one (BIQ). *Chem Asian J* 2011;6(3):856–62.
- [25] Kan B, Zhang Q, Li M, Wan X, Ni W, Long G, et al. Solution-processed organic solar cells based on dialkylthiol-substituted benzodithiophene unit with efficiency near 10%. *J Am Chem Soc* 2014;136(44):15529–32.
- [26] Mishra A, Bäuerle P. Small molecule organic semiconductors on the move: promises for future solar energy technology. *Angew Chem Int Ed* 2012;51(9):2020–7.
- [27] Ye L, Zhang S, Zhao W, Yao H, Hou J. Highly efficient 2D-conjugated benzodithiophene-based photovoltaic polymer with linear alkylthio side chain. *Chem Mater* 2014;26(12):3603–5.
- [28] Hou J, Chen H, Zhang S, Chen RI, Yang Y, Wu Y, et al. Synthesis of a low band gap polymer and its application in highly efficient polymer solar cells. *J Am Chem Soc* 2009;131(43):15586–7.
- [29] Chen H, Huang H, Huang X, Clifford JN, Forneli A, Palomares E, et al. High molar extinction coefficient branchlike organic dyes containing di(p-tolyl)phenylamine donor for dye-sensitized solar cells applications. *J Phys Chem C* 2010;114(7):3280–6.
- [30] Ni W, Li M, Wan X, Feng H, Kan B, Zuo Y, et al. A high-performance photovoltaic small molecule developed by modifying the chemical structure and optimizing the morphology of the active layer. *RSC Adv* 2014;4:31977–80.
- [31] Li G, Kang C, Gong X, Zhang J, Li W, Li C, et al. 5,6-Difluorobenzothiadiazole and silafluorene based conjugated polymers for organic photovoltaic cells. *J Mater Chem C* 2014;2(26):5116–23.
- [32] Yan W, Hong C, Long G, Yang Y, Liu Z, Bian Z, et al. Synthesis, crystal structures and photophysical properties of novel boron-containing derivatives of phenylene with bright solid-state luminescence. *Dyes Pigments* 2014;106:197–204.
- [33] Mihailtchi VD, Xie HX, de Boer B, Koster LJA, Blom PWM. Charge transport and photocurrent generation in poly(3-hexylthiophene):methanofullerene bulk-heterojunction solar cells. *Adv Funct Mater* 2006;16(5):699–708.
- [34] Mei C, Liang L, Zhao F, Wang J, Yu L, Li Y, et al. A family of donor–acceptor photovoltaic polymers with fused 4,7-dithienyl-2,1,3-benzothiadiazole units: effect of structural fusion and side chains. *Macromolecules* 2013;46(19):7920–31.